Microchemical Journal 207 (2024) 112091

Contents lists available at ScienceDirect

Microchemical Journal

journal homepage: www.elsevier.com/locate/microc

Uric acid detection by hydrogen peroxide independent biosensors: Novel insights and applications

M. Koch [a], Y.E. Silina [b,*]

[a] INM – Leibniz Institute for New Materials, Saarbrücken, Germany
[b] Saarland University, Institute of Biochemistry, Saarbrücken, Germany

ARTICLE INFO

Keywords:
Uric acid
Uricase
Electrodeposition
Biochemical route
Electrooxidation
Fermentation samples

ABSTRACT

Uric acid (UA) is one of the most electroactive low molecular weight compounds that can be electrochemically oxidized on the surfaces of numerous noble and non-noble electrocatalysts under applied polarization. Consequently, enzymatic determination of UA in model and real samples is complicated by possible interference between electrochemical and biochemical routes.

Herein, a novel strategy for amperometric enzymatic hydrogen peroxide independent UA sensing at low concentrations (*e.g.,* below 50 μM) is proposed. The UA-sensitive strategy relies on the use of screen printed electrodes modified by an electrodeposited hybrid functional sensing film comprising a non-noble electrocatalyst, a bioorganic layer containing enzyme uricase (UOx), and data acquisition enabling the biochemical transformation of UA to be distinguished from the electrochemical oxidation route. Performed selectivity test utilizing adenine, xanthine, urea, ascorbic acid, ethanol and glycerol did not reveal interferences during detection of UA.

This proposed approach was tested for UA detection in model and fermentation samples. The quantitative results obtained in fermentation samples were validated through optical oxygen mini sensor studies and fluorescence-based bioassays.

1. Introduction

Uric acid (UA), a nitrogen compound derived from purine degradation, has metabolic importance in both biochemistry and biotechnology. [1] UA levels often indicate essential alterations in purine metabolism, and in cellular transport and storage mechanisms.

The conventional analytical approaches used for analysis of UA in model and real biological samples include liquid chromatography-based and enzymatic assays combined with spectrophotometric and fluorometric detection.[2,3] However, these approaches are time consuming, have limited dynamic range and require additional multi-stage sample preparation procedures and complex data interpretation.

In contrast, electrochemical approaches such as amperometric biosensing enable a rapid analysis with excellent sensitivity.[4] A wide range of enzymatic biosensors have been proposed for determination of UA in blood, urine and food samples, with varying success.[5–7] Most amperometric biosensor designs use enzyme uricase, binding agents (Nafion or carboxymethyl cellulose) and inorganic mediators (Prussian Blue) [8,9] or electrocatalysts (noble metal nanostructures).[10,11] Unfortunately, the lack of universal instrumentally controlled synthesis of functional sensing biolayers in enzymatic hydrogen peroxide-sensitive amperometric biosensors substantially affects the synthesis reproducibility and analytical merit in electrochemical assays. Thus, numerous multi-step and multi-technological approaches have been utilized for preparation of functional sensing films of biosensors for UA detection, *e.g.,* covalent linkage, drop-casting layer-by-layer, precipitation, thermal decomposition and physical adsorption.[12–16].

Non-enzymatic UA sensing is primarily based on the use of carbon nanomaterials,[17,18] transition metals [19–23] or their oxides, [5,24] and enables direct electrooxidation of UA in aqueous solutions.[25,26] In this case the oxidation peak current is directly proportional to the concentration of UA. In non-enzymatic sensing the step associated with enzyme immobilization is absent, thus minimizing errors arising in the preparation stage of functional biolayers. However, these non-enzymatic electrochemical sensors drawbacks of interference arising from the oxidation of electroactive substances present in the same sample, cross-sensitivity and low selectivity. Therefore, despite simplicity and economy of non-enzymatic electrochemical UA sensors,

* Corresponding author at: Institute of Biochemistry, Saarland University, Saarbrücken, Campus B 2.2, room 317, Germany.
E-mail addresses: yuliya.silina@gmx.de, yuliya.silina@uni-saarland.de (Y.E. Silina).

https://doi.org/10.1016/j.microc.2024.112091
Received 23 August 2024; Received in revised form 29 September 2024; Accepted 31 October 2024
Available online 1 November 2024

their insufficient specificity and selectivity remain a big issue.

Moreover, future progress in UA non-enzymatic and enzymatic sensing will prioritize trace-level analysis. Therefore, the development of alternative chemical and biochemical logic systems [27] and measurement strategies would provide new opportunities for reliable UA detection in real objects, *e.g.,* fermentation samples.

Herein, functional sensing layers and measurement strategy for hydrogen peroxide independent UA detection in microbial cells supernatants (*S. cerevisiae* yeasts, *E.coli* bacterial cells) at low concentrations (below 50 μM) is proposed.

The novelty of this study relies on a novel detection principle of amperometric uric acid (UA) biosensing (i); revealed mechanistic aspects underlying non-enzymatic amperometric sensing of UA on the surfaces of the most commonly used electrocatalysts (ii) and a novel design of amperometric UA biosensor based on an electrodeposited sensing film produced by fully instrumentally controlled synthesis (iii).

2. Experimental part

2.1. Chemicals and materials

H_2PdCl_4, $(NH_4)_2HPO_4$, $Na_2HPO_4{\cdot}12H_2O$, 25 % NH_4OH, ethanol (EtOH), glycerol solution (85 %), ascorbic acid (AA), KOH pellets, uric acid (UA), adenine, xanthine, urea, 5 % Nafion solution, $CuSO_4$, yeast fermentation HC complete medium (Hartwells Complete medium) and M9 *E. coli* medium, uricase (UOx, from *Bacillus fastidiosus*) were received from Merck (Darmstadt, Germany). An Amplex™ Red Uric Acid/Uricase Assay Kit was obtained from Thermo Fisher Scientific (Massachusetts, US).

Screen printed electrodes (SPEs) on ceramic substrates were obtained from DropSens (Metrohm, Germany). The electroanalytical performance of the following electrodes toward UA was evaluated: commercial graphene oxide (GO, DRP-110DGPHOX), commercial platinum structures (Ref 550-Pt), commercial gold particles (Ref 220 AF, Au-AT), gold particles (Ref 220 BT, Au-BT) and commercial ruthenium oxide particles (Ru_xO_y, DRP-810-U50).

Palladium, nickel and copper particles were electrodeposited on the surface of SPE modified by graphene oxide (SPE/GO). Briefly, Pd-particles were formed from the basic electrolyte at a cathodic current of -2.5 mA for 30 s.[28] Copper and nickel particles were electrodeposited from 30 mM $CuSO_4$ or $NiSO_4$ electrolytes at −0.5 mA for 30 s. The procedure was repeated in triplicate.

2.2. Formation of the sensing hybrid Cu-NPs/UOx/Naf layer

A hybrid enzymatic layer consisting of UOx, Nafion and copper particles (as a case study) was produced on the SPE/GO surface. Multiple electrolyte was prepared by mixing of $CuSO_4$ with 5 % Nafion (Naf) and UOx at a concentration of 3 mg/mL (UOx was dissolved in phosphate buffer, pH 9) in a ratio of 1:1:1 *(v/v/v)*. Electrodeposition of the hybrid layer was conducted on the SPE/GO surface at -0.5 mA for 30 s. After formation of the sensing Cu-NPs/UOx/Naf layer the electrodes containing enzymes were carefully washed with DI water and stored in a refrigerator at + 4 °C.

2.3. Electrochemical studies

The electrochemical performance of SPEs modified by various sensing layers in a 150 μL droplet of UA model solutions or real fermentation medium/supernatants was explored on a one-channel PalmSens4 potentiostat (PalmSens, Utrecht, The Netherlands) in cyclic voltammetry (CV) mode in the range from -0.4 V to 0.6 V and scan rate of 50 mV/s.

For evaluation of the selectivity of the developed electrodes, their responses were recorded in amperometric (AM) mode at an applied voltage equal to 0.22 V (unless otherwise specified). Calibration of the electrodes was conducted in a multi-step amperometric mode (MAM) as follows: level 1 polarization in the cathodic range (supporting surface cleaning between cycles) at -0.1 V held for 60 s followed by polarization at level 2 for signal read-out at 0.22 V for 30 s. The first signal read-out in a 150 μL droplet of test solution was conducted 90 s after the start; the MAM procedure was subsequently repeated for 180 s and 270 s.

Calibration of electrodes in UA solutions was performed through the external standard approach (ESTD) at pH 9.

2.4. Cell cultivation/supernatants collection

Yeast colonies (*S. cerevisiae,* strain BY4742) were cultivated in flasks in HC complete medium at 32 °C for 24 h. After cultivation and measurement of the optical density (OD_{600}) on an Ultrospec 10 instrument (Thermo Fisher Scientific), cells were removed from the medium by centrifugation at 13000 rpm for 10 min. The obtained supernatant that had been in contact with cells was used for subsequent analysis.

The same supernatant preparation procedure was conducted for *E. coli* cells cultivated in M9 medium at 37 °C for 2, 12 and 24 h.[29] Before analysis the supernatant pH was adjusted to 9 ± 0.05 with phosphate buffer (with pH 12).

UA recovery in fermentation samples (yeast and *E. coli* supernatants) were determined as follows: UA standard solutions (5 μM, 10 μM and 100 μM) were spiked into 1/2 diluted by phosphate buffer fermentation samples to achieve pH 9 ± 0.05, and the amperometric responses were compared with the initial signals [4,30].

2.5. Uricase assay KIT

For validation of the content of UA present in supernatants of microbial cells, an Amplex™ Red Uric Acid/Uricase KIT assay from Thermo Fisher Scientific was used. Before addition of KIT reagents the tested supernatants and blank solutions were diluted in a ratio of 1 to 5 with buffer. All reactive reagents and test solutions were stored on ice, protected from light and used promptly. Measurements were conducted at 585 nm in fluorescence microplates on an FP-8500 spectrofluorometer (Jasco, Tokyo, Japan).

2.6. Scanning electron (SEM), transmission electron (TEM) microscopy and energy dispersive X-ray (EDX) analysis

The morphology of the sensing layers of SPEs was studied by scanning electron microscopy (SEM) in high vacuum mode on a FEI (Hillsboro, OR, USA) Quanta 400 FEG equipped with an EDAX (Mahwah, NJ, USA) Genesis V 6.04 X-ray module at an accelerating voltage of 10 keV. TEM measurements of the hybrid sensing layer were performed utilizing a JEOL (Akishima, Japan) JEM-2100 microscope. Therefore, the surface layer of the electrode was scratched using sandpaper and the resulting pieces were transferred to a holey carbon supporting TEM grid (Plano, Wetzlar, S147-4). Bright field TEM images were acquired at 200 kV accelerating voltage using a Gatan (Pleasanton, CA, USA) Orius SC-1000 CCD camera.

2.7. Oxygen minisensor studies

Limitations of conventional analytical methods (*e.g.,* FT-IR, Raman, XRD, etc.) applied characterization of nano-dimensional sensing layers electrodeposited on the surface of SPEs were highlighted in several studies.[31,32] However, due to the presence of a biocomponent/enzyme (UOx) in the design of the sensing layer it is possible to control the efficiency of electrodeposition by approaches used in biotechnology. [33] Thus, work of UOx is based on oxygen consumption; hence, the biochemical transformation of the substrate/UA can be monitored through the analysis of the amount of consumed oxygen. For evaluation of the intensity of oxygen consumption in the presence of UOx, the oxygen concentration ($\mu mol{\cdot}L^{-1}$) in test solutions was monitored with an

OXR430 needle oxygen minisensor (Pyro Science GmbH, Aachen, Germany) according to a previously reported protocol. [34].

To verify the electrodeposition of UOx from the multiple electrolyte solution on the SPE/GO surface and its retained biochemical activity, oxygen consumption was monitored directly on the electrode modified by the hybrid sensing film in a 150 μL droplet of UA at pH 9. This method enabled the visualization of UA biochemical transformation.

3. Results and discussion

3.1. Electroanalytical performance of selected noble and non-noble electrocatalysts in model UA solutions: Potential superiority of the electrochemical route of UA oxidation vs the biochemical route

Typically, amperometric biosensor design development begins with the choice of electrocatalyst followed by performance testing in solutions comprising fermentation reaction products. If oxidases are used, the performance of electrocatalysts should first be evaluated in the presence of H_2O_2 as a product of a biochemical reaction between the target oxidase (*e.g.,* glucose oxidase, lactate oxidase or uricase) and substrate (glucose, lactate or UA, respectively). Ideal electrocatalysts should be insensitive to the target substrate while showing high efficiency towards the electrochemical transformation of hydrogen peroxide as a product of the enzymatic reaction.

Unexpectedly, all tested electrocatalysts in this study showed a response in model UA solutions (substrate) even in the absence of target enzyme (UOx), Fig. 1.

Thus, regardless of the type of electrocatalyst used in electrodes sensing layers electrochemical oxidation of UA occurs with varying efficiency. Simultaneously, non-desirable and non-controlled electrochemical oxidation of UA can result in suppression the biochemical reaction in the presence of a specific enzyme (UOx). In the worst case, the elevated signal might be mistakenly attributed to the biochemical reaction with UA recorded from the electrode with immobilized UOx.

In biosensors with hybrid layers containing both UA-sensitive electrocatalysts and UOx, at least two parallel routes (electrochemical (*i*) and biochemical (*ii*) oxidation) of UA transformation can occur. In the case of noble metal electrocatalysts, an additional concurrent reaction related to oxidation of hydrogen peroxide (*iii*) as a product of the enzymatic reaction can occur (described in the section below).

3.2. Hydrogen peroxide dependent electrodes are unlikely to enable for UA determination in fermentation samples

First, we optimized experimental conditions supporting enzymatic transformation of UA, such as the pH. Briefly, according to the results of oxygen mini-sensor studies, the uricase (UOx) solution showed favorable biochemical activity in the presence of UA at pH 9, **ESI, Fig. S2A**. At pH 9, UA exists in deprotonated form as the urate anion [35,36] thus influencing its interaction (*i.e.*, adsorption efficiency) [37] with the electrode material/electrocatalyst. Notably, the use of UOx in the sensing layer design supported high selectivity of UA sensing at pH 9 even in the presence of analogues, *i.e.*, other purines (**ESI, Fig. S2B**). A further increase of the pH might cause deactivation of UOx.[38,39].

Enzymatic amperometric determination of UA relies on the following route:[7]

$$\text{Uric acid} + 2H_2O + O_2 /(UOx) \rightarrow \text{allantoin} + CO_2 + H_2O_2 \quad (1)$$

Because of oxygen electroreduction on the surfaces of the most frequently tested electrocatalysts in the cathodic range of potentials, amperometric detection of UA according to oxygen consumption (reaction (1)) is doubtful.[40] Simultaneously, the amount of H_2O_2 formed as a product of enzymatic reaction proportional to UA biochemical transformation can readily be monitored on the electrode:

$$H_2O_2 \rightarrow O_2 + 2H^+ + 2e- \quad (2)$$

Thus, the electrocatalysts frequently applied in biosensors design for UA detection should be highly sensitive to oxidation of H_2O_2.

Our previous studies [37,40] have demonstrated the excellent activity of electrodeposited palladium-based electrocatalysts used in the design of oxidase-based electrodes sensing layers for H_2O_2 electrooxidation at pH 7. However, at alkaline pH, the performance of the electrocatalysts most active toward H_2O_2 may substantially decrease. This possibility was validated in an experiment utilizing palladium nanoparticles (Pd-NPs), H_2O_2 and UA, Fig. 2. Briefly, the electrooxidation ability of noble metal-based electrocatalysts (shown for electrodeposited Pd-NPs as a case study) at alkaline pH was much higher toward UA than H_2O_2. Therefore, superior electrooxidation of UA would be achieved with noble metal based electrocatalysts rather than enzymatic biochemical transformation accompanied by H_2O_2 release.

Consequently, hydrogen peroxide sensitive electrocatalysts cannot effectively support UA biosensing in model or real fermentation samples (electrochemical transformation of UA would first occur on the electrode surface).

Moreover, the concentration of UA in the supernatants of the fermentation samples, as tested with an Amplex™ Red conventional biochemical assay was very low, and did not exceed 17 μM, see **ESI, Table S1**. Therefore, the amount of hydrogen peroxide (formed as an enzymatic reaction product) would be also insufficient and thus, in the presence of numerous interfering electroactive species would be unlikely to be reliably detected by noble metal based electrocatalysts in fermentation samples. More importantly, the simultaneous cross-response of noble metal electrocatalysts to H_2O_2 and UA would certainly affect the performance of electrodes in a non-controlled manner.

In terms of practical applications, a proper UA electrocatalyst should at least exclude the reaction with hydrogen peroxide. Simultaneously, apart from H_2O_2 no other electroactive compounds are formed in the biochemical reaction between UOx and UA, thus causing possible problems during signal detection.

As a solution, the use of electrocatalysts that are hydrogen peroxide insensitive and simultaneously highly sensitive to UA could be explored. For that case, an original data acquisition during enzymatic UA transformation is described in subsequent sections.

3.2.1. Choice of UA-sensitive electrocatalysts and identification of optimal operating conditions

In choosing hydrogen peroxide independent electrocatalysts, one criterion must be considered: higher electrocatalyst response to UA is ideal. In this regard, because of the exclusive sensitivity of electrodeposited Cu-NPs to UA, as compared with analogues (Fig. 1), in our subsequent experiments, the design of the functional sensing layers was based on this electrocatalyst.

Notably, electrodes based on electrodeposited Cu-NPs and Ni-NPs were absolutely insensitive to H_2O_2 and allantoin electrooxidation at alkaline pH, even with high applied concentrations (as shown in **Fig. S3** for Cu-NPs modified SPE/GO as an example). Hence, no concurrent reactions to H_2O_2 would be expected during UA electrooxidation regardless of the measurement principle used, *e.g.,* non-enzymatic or enzymatic sensing. In addition, the maximum oxidation peak of UA on Cu-NPs was approximately about ~ 0.20 – 0.22 V much lower than the ~ 0.3 – 0.7 V for other electrocatalysts explored in this study (Fig. 1**,A-I**) and thus would affect electroanalytical performance. Indeed, the electrode based on Cu-NPs showed an excellent linear dynamic range (LDR) to UA, *e.g.* from 2.5 μM to 2 mM, and had a limit of detection (LOD)/ equal to a limit of quantification (LOQ) of 2.5 μM, Fig. 3.

Furthermore, tandem of oxygen minisensor and electrochemical (CV) studies revealed that a biochemical reaction using UOx readily competed with the electrochemical transformation of UA in terms of

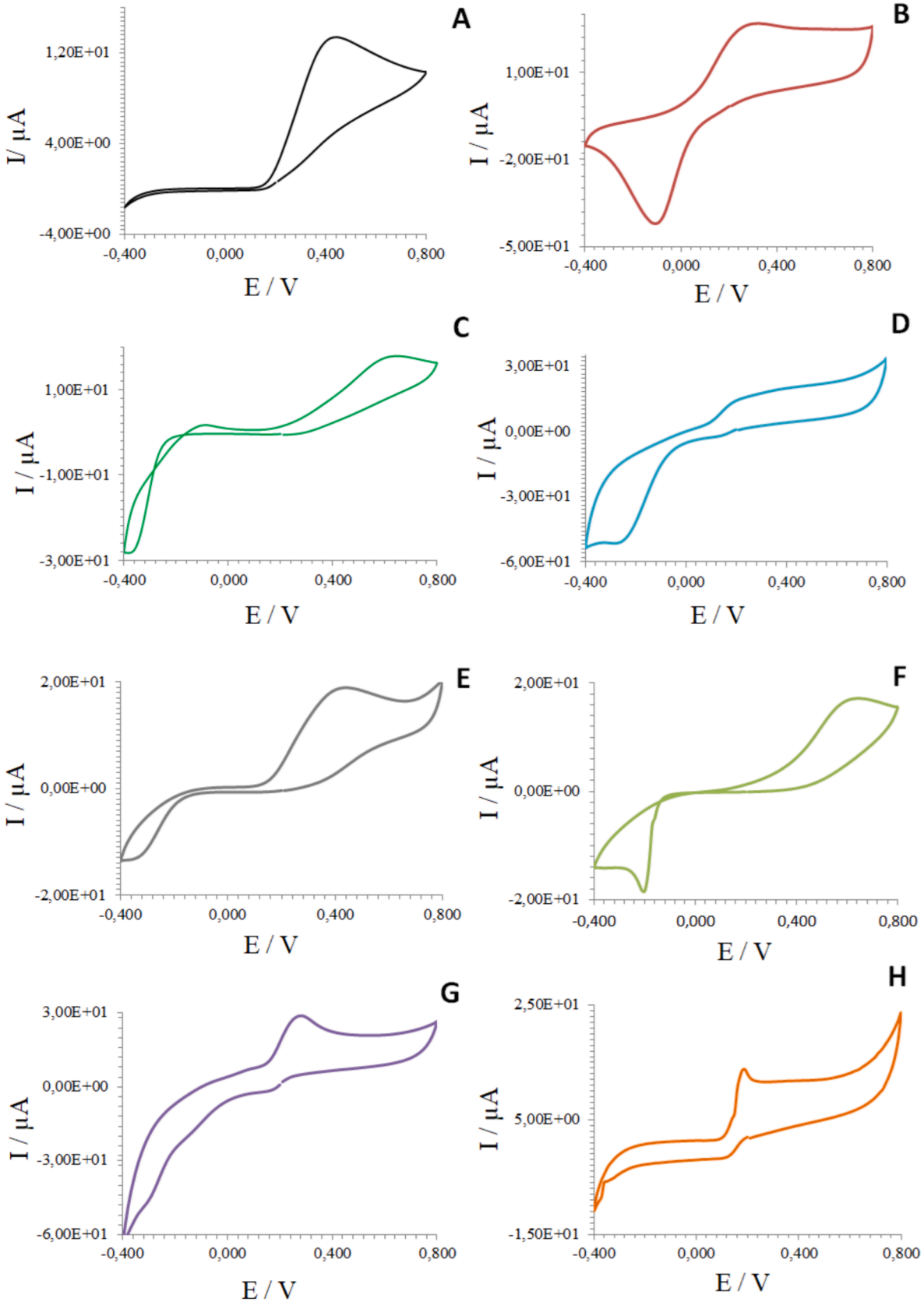

Fig. 1. (**A** – **I**) CV plots (second scans shown) recorded in a droplet of 1 mM of UA at 50 mV/s from the following SPEs: **A** – commercial SPE/GO, **B** – commercial SPE/Pt, **C** – commercial SPE/Au-AT, **D** – commercial SPE/GO with electrodeposited Pd-NPs, **E** – commercial SPE/Au-NPs (Au-BT), **F** – commercial SPE/Ru_xO_y, **G** – commercial SPE/GO with electrodeposited Cu-NPs, **H** – commercial SPE/GO with electrodeposited Ni-NPs. The measurements were conducted in triplicate with the same results. *Note:* SEM images of the tested electrocatalysts are summarized in **ESI, Fig. S1**.

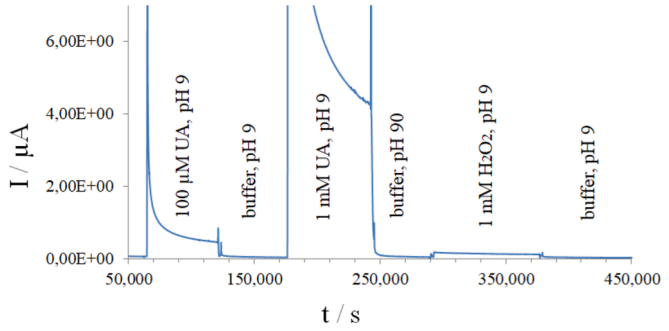

Fig. 2. Selectivity test performed at pH 9 on an electrode modified by electrodeposited Pd-NPs (shown for the structure D in Fig. 1, see also SEM image of Pd-NPs, ESI, Fig. 1Ď) in AM mode at an applied voltage of 0.22 V.

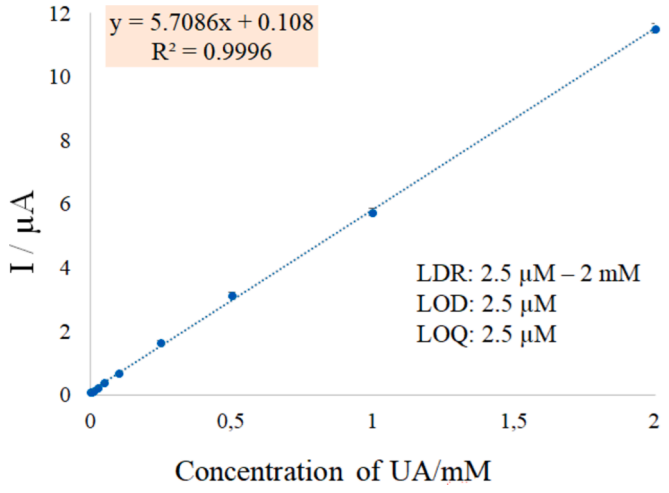

Fig. 3. Calibration curve of UA obtained in buffer (pH 9) through the ESTD approach in MAM from SPE/GO modified by electrodeposited Cu-NPs: level 1 at -0.1 V hold for 60 s, level 2 (signal read-out) at 0.22 V at 30 s (total signal run 90 s). The measurements were conducted in triplicate; mean value ± SD for each UA concentration is shown.

speed. Briefly, after only 300 s from the start of the biochemical reaction, complete biochemical conversion of the substrate/UA to the products (allantoin and H_2O_2) was observed in the solution, **ESI,** Fig. S4**A**. This finding indicated a slow biochemical oxidation speed of UA by the tested enzyme (UOx from *Bacillus fastidiosus*). At the same time, the speed of the biochemical reaction on the electrode at the applied polarization slightly differed compared to solutions.

Our CV studies (**ESI,** Fig. S4**B**) revealed the remaining amount of non-biochemically transferred UA in the presence of aqueous UOx on the electrode as a result of electrochemical oxidation after completion of the first CV run (70 s, UA was still visualized in CV plots). From a practical viewpoint this observation would suggest substantial difficulties during data acquisition and signal read-out earlier than 70 s. Therefore, for determination of UA with Cu-NPs based electrodes in the presence of UOx, we used MAM mode supporting signal read-out in the same droplet in triplicate at 90 s, 180 s and 270 s (60 s cathodic polarization, 30 s – anodic signal read-out, see *Experiment*).

Notably, the speed rates and behavior of UA electrooxidation on the surfaces of pure electrodeposited Cu-NPs in the absence of UOx did not substantially vary among scans (**ESI,** Fig. S4**C**) thus highlighting the possibility of distinguishing the biochemical transformation route of UA from electrochemical oxidation (described in the next sections).

3.3. Tandem non-enzymatic UA-sensing and biosensing: Distinguishing electrochemical from biochemical reactions on the electrode with the hybrid layer

Even when highly UA-sensitive electrocatalysts are used in the design of electrodes, non-enzymatic UA determination in model and fermentation samples is challenging; thus, a wide spectrum of potentially electroactive compounds at the same pH may be present in supernatants at high concentration (for example, glycerol (50 – 80 mM) [30,41,42]) thus affecting UA analysis at alkaline pH (*e.g.,* at low concentration range (µM), see Table S1) in the absence of specific enzymes.

Therefore, on the next step, UOx was electrodeposited from the multiple electrolyte solution (containing 1 mg/mL of UOx) together with Cu-NPs and Nafion (was used to prevent rapid elution of water soluble enzyme) on the SPE/GO surface (see *Experiment*).

The morphology of the hybrid sensing electrodeposited Cu-NPs/UOx/Naf film was represented by a thin bioorganic layer (**ESI,** Fig. S5**A**). The entrapped inorganic Cu-NPs within the bioorganic layer were visualized by TEM (**ESI,** Fig. S5**B**). EDX analysis (**ESI, Fig, 5C**) confirmed the presence of small amount of Cu (corresponds to Cu-NPs), S-line (corresponds to Nafion) and N-line (corresponds to biocomponent, UOx) in the spectra recorded from the hybrid layer. Electrodeposition of copper from multiple electrolytes often leads to the formation of nanodimensional Cu-NPs.[43,44] Although the good reproducibility of nanoscale films is usually difficult to maintain, in our case, because of the fully instrumentally controlled electrodeposition synthesis of sensing layers, the reproducibility of the basic line recorded from the hybrid electrodes across runs and batches was very high, **ESI,** Table S2.

The evolution of the signal read-out recorded from electrodes based on Cu-NPs and UOx summarized in Fig. 4 (shown for 1 mM of UA, to achieve pronounced trends).

By changing the functional film from individual electrodeposited Cu-NPs (Fig. 4a) to the hybrid layer (Fig. 4b), a noticeable signal decrease corresponding to enzymatic UA electrooxidation occurred. This simple experiment demonstrated the successful electrodeposition of UOx from multiple electrolyte on the SPE/GO surface under the applied polarization. The more UOx present on the electrode, the less signal intensity/anodic current recorded from the electrode (Fig. 4c). This relationship was also confirmed for electrodeposited hybrid films according to the amounts of UOx used in multiple electrolyte, **ESI,** Fig. S6. Briefly, the highest anodic signal corresponding to the remaining free amount of electrochemically oxidized UA on Cu-NPs was observed for the electrode with a minimum amount of electrodeposited UOx (0.3 mg/mL), the lowest – for maximum amount of UOx (3 mg/mL in stock) used for the preparation of multiple electrolyte solution.

To exclude the influence of the non-conductive nature of the immobilized bioorganic component [15] on the observed decrease in the current (Fig. 4b) in the presence of UA (Fig. 4a), we deactivated UOx in the structure of sensing layer (Fig. 4b). For this goal, the electrode with electrodeposited hybrid Cu-NPs/UOx/Naf film was heated to 70 °C for 20 min. After the heating procedure the physical–chemical nature of the sensing layer as well as the electroactive surface area remained unaffected, however, UOx was no longer biochemically active (*e.g.,* was unable to oxidize UA via the biochemical route).

Furthermore, the electroanalytical performance of this electrode with deactivated UOx was tested again in UA solutions under the same pH and electrochemical conditions. Interestingly, after deactivation of UOx the responses of hybrid electrodes in a droplet of UA became similar regardless of the amount of primary co-deposited UOx, Fig. 5 (shown for 1 mg/mL UOx and 3 mg/mL UOx used in multiple electrolytes, see also Fig. S6, **ESI**).

This simple model experiment indicated that the reason for the decrease of the anodic signal in UA solutions was actually caused the activity of the enzyme (UOx) in the hybrid sensing layer. Moreover, this experiment highlighted the possibility of switching the signal read-out

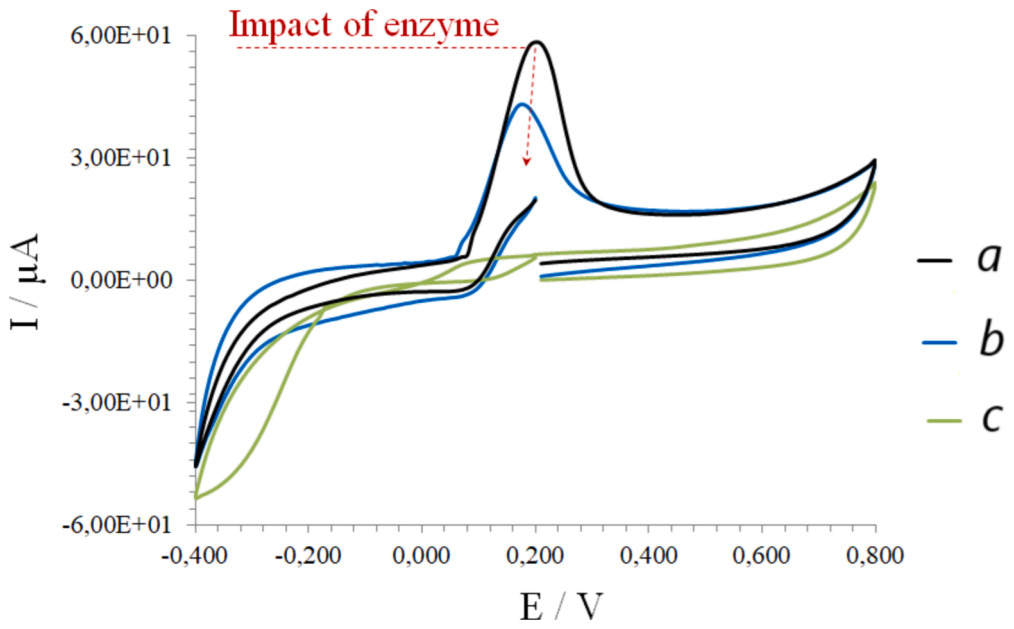

Fig. 4. CV plots recorded at 50 mV/s in a droplet of 1 mM of UA at pH 9 from: *a* – SPE/GO modified by electrodeposited Cu-NPs; *b* – SPE/GO with an electrodeposited hybrid Cu-NPs/UOx/Naf layer; *c* – electrode (*a*) with addition of aqueous UOx into the droplet. The measurements were performed in triplicate and yielded the same results.

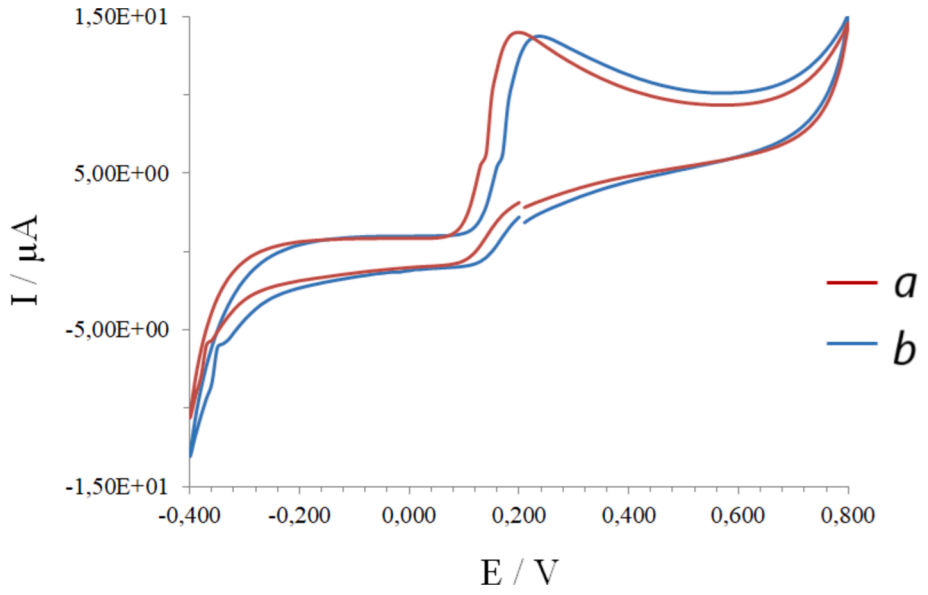

Fig. 5. CV plots recorded at 50 mV/s and pH 9 from Cu-NPs/UOx/Naf modified electrodes after heating at 70 °C for 20 min in a droplet of 1 mM of UA: *a* – amount of UOx in multiple electrolyte at 1 mg/mL; *b* – amount of UOx in multiple electrolyte at 3 mg/mL.

mode from enzymatic (using UOx) to non-enzymatic (using individual electrodeposited Cu-NPs) in the framework of the same electrode.

3.4. *Validation of enzymatic reactions in the hybrid sensing layer*

Notably, oxygen related processes on the surfaces of electrodes modified by the hybrid electrodeposited Cu-NPs/UOx/Naf film in the presence of low amounts of UA differed from those on the surface of individual Cu-NPs, Fig. 6. Thus, during scanning of the electrode based on Cu-NPs, the oxygen content in a droplet of 10 μM of UA was maintained at almost the constant level, *viz.* 260 – 270 μmol/L, Fig. 6a. In contrast, pronounced oxygen consumption (Fig. 6b) with clear maxim matching the anodic range of potentials in CV during all three cycles was observed on the surfaces of the electrode with an electrodeposited hybrid Cu-NPs/UOx/Naf layer. This trend highlighted the interaction of UOx with 10 μM UA according to formula (*1*).

Interestingly, after the heating of the electrode modified by Cu-NPs/UOx/Naf resulted in deactivation of UOx, the oxygen related processes occurring on the electrode surface switched again (Fig. 7c) to that occurring on the intact Cu-NPs, Fig. 6a. In that case, non-enzymatic UA sensing would be expected.

Analytical performance of electrodes modified by a hybrid sensing layer

Selectivity test using alternative purines (adenine, xanthine) and compounds possibly present in fermentation samples, *e.g.,* ethanol, glycerol and urea did not reveal any interference in the detection of UA

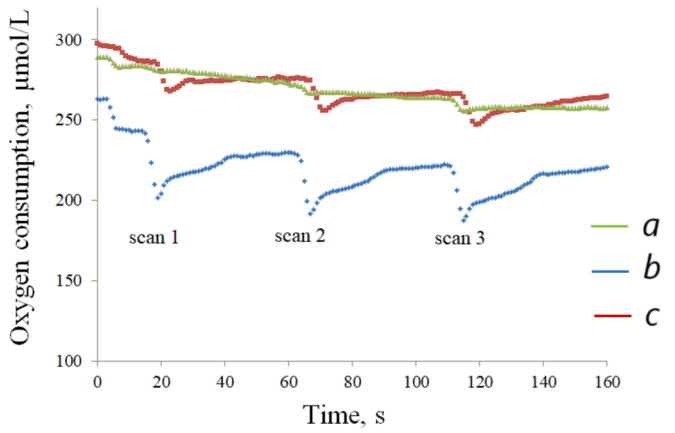

Fig. 6. Dynamic oxygen mini-sensor responses recorded in a droplet of 10 µM of UA at pH 9 from the following electrodes: *a* – individual electrodeposited Cu-NPs; *b* – hybrid electrodeposited Cu-NPs/UOx/Naf (1 mg/mL UOx in the multiple electrolyte); *c* – electrode (*b*) after heating at 70 °C for 20 min. *Note:* during signal recording the electrodes were scanned three cycles in CV mode from −0.4 V to 0.8 V at a scan rate of 50 mV/s.

by electrode modified by hybrid sensing Cu-NPs/UOx/Naf film, Fig. 7. Notably, in AM mode no response to the diluted yeast supernatant (collected from cells with OD 4.9) was recorded from this electrode, thus probably indicating the absence of UA in the tested fermentation sample.

However, given the lower UA concentration (below 20 µM) present in fermentation samples (**ESI**, **Table S1**) than the concentrations tested in Fig. 7 (0.1 – 1 mM), the possibility of a biochemical UA transformation resulting in a current decrease (according to Fig. 4) and false negative result could not be excluded. Thus, although a sample might originally contain UA, after interaction with UOx on the electrode, UA could be converted into non-electrochemically active products that cannot be detected in AM mode.

To verify this possibility, we assessed the electroanalytical performance of the electrode modified by a Cu-NPs/UOx/Naf layer in MAM mode in model and real fermentation solutions spiked with low amount of UA, *e.g.,* 5 – 100 µM. The analytical performance of this electrode was compared with results recorded from the electrode modified by individual electrodeposited Cu-NPs. Remarkably, the calibration of the electrode modified by a hybrid by Cu-NPs/UOx/Naf film was impossible up to 50 µM of UA. Briefly, the obtained currents were below the basic line corresponding to the solution without addition of UA, **ESI, Fig. S7A** (shown for model solutions). This effect was easily explained by interaction of the UOx present in the design of sensing hybrid layer with a low concentration added UA. That is, false negative results could easily have been recorded from the electrode modified by the hybrid UOx-containing layer (spiked values in sample, Table 1, Table 2).

Simultaneously, false positive results could be obtained from the electrode based on individual Cu-NPs (because of cross-selectivity of Cu-NPs with other electroactive compounds possibly present in fermentation samples, thus resulting in signal suppression or enhancement). The amount of UA in tested yeast supernatant was 4.08 ± 0.05 determined through a bioassay (**Table S1**) *vs* 12.26 ± 0.01 found with an electrode modified by Cu-NPs (Table 1) indicating matrix enhancement, whereas the amount of UA determined in an *E. coli* sample was 9.01 ± 0.04 (**Table S1**) *vs* 15.46 ± 0.01, highlighting matrix suppression (Table 2).

Regarding the enzymatic biosensing route of UA, the obtained results enabled rapid screening of fermentation samples for the presence of UA below or above 50 µM (qualitative and semi-quantitative test). If the concentration of UA exceeded 50 µM, the signal corresponded to its residual electrooxidation on Cu-NPs in a non-enzymatic manner. If the sample contained a low amount of UA (below 50 µM), no current increase would be expected from the electrode modified by hybrid electrodeposited Cu-NPs/UOx/Naf (because of biochemical oxidation of UA).

3.5. Amperometric enzymatic quantification of UA

During this investigation, an option enabling quantitative biosensing of UA at very low concentration range (below 20 µM) using Cu-NPs/

Table 1
Selected recoveries UA spiked in yeast supernatant (OD = 4.9 as a case study, cells were cultivated for 24 h) obtained from the tested electrodes by conventional ESTD.

Sensing layer	Calibration formula, R^2	UA, µM	Spiked UA, µM	Found UA, ±SD, µM	RSD, %
Cu-NPs	y = 0.005x + 0.0207, R^2 = 0.999	12.26 ± 0.01	5.00	15.86 ± 0.11	5.41
			10.00	19.86 ± 0.01	3.76
			100.00	109.86 ± 0.03	2.17
Cu-NPs /UOx/ Naf	y = 0.0048x + 0.429*R^2 = 0.958	– **	5.00	–	–
			10.00	–	–
			100.00	42.04 ± 0.04	5.26

* calibrated from 50 to 150 µM;
** UA was not found.

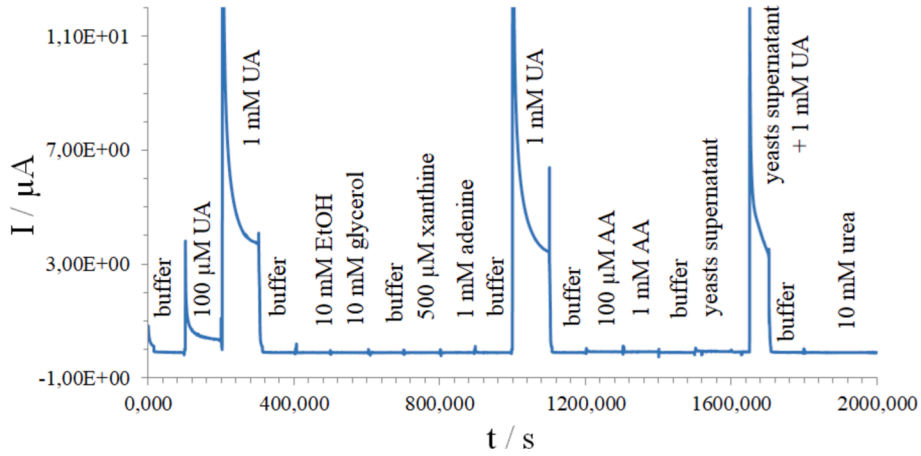

Fig. 7. Results of selectivity test performed in AM mode for SPE/GO modified by a hybrid electrodeposited Cu-NPs/UOx/Naf layer. *Note:* UA – uric acid, AA – ascorbic acid. pH of all tested solutions was set at 9 ± 0.2 and signal recording was conducted in AM mode every 200 s.

Table 2
Selected recoveries UA spiked in *E. coli* supernatant (OD = 3.1 as a case study, cells were cultivated for 12 h) obtained from the tested electrodes by conventional ESTD.

Sensing layer	Calibration formula, R^2	UA, μM	Spiked UA, μM	Found UA, ±SD, μM	RSD, %
Cu-NPs	y = 0.005x + 0.0207, R^2 = 0.999	15.46 ± 0.01	5.00	8.46 ± 0.06	3.76
			10.00	10.26 ± 0.05	9.90
			100.00	91.50 ± 0.63	9.11
Cu-NPs /UOx/ Naf	y = 0.0048x + 0.429*R^2 = 0.958	– **	5.00	–	–
			10.00	–	–
			100.00	60.47 ± 0.03*	4.87

* calibrated from 50 to 150 μM;
** UA was not found.

UOx/Naf modified electrode was identified. Thus, negative calibration of this electrode based on a current decrease caused by formation of products of the enzymatic reaction (allantoin, hydrogen peroxide and carbonates) non-electroactive on Cu-NPs (see **ESI, Fig. S3**) could readily be used. For example, carbon dioxide (a product of the enzymatic reaction between UOx and UA, see formula (*1*)) at alkaline pH results in the formation of carbonates.[45] With an increase in UA concentration from 5 μM to 20 μM, the amount of non-electroactive products formed on the sensing layer also increased, thus masking the electroactive surface area of the electrode and resulting in a decline in the signal below the basic line (**ESI, Fig. S7A**).

The presence of UOx in the design of the Cu-NPs/UOx/Naf sensing layer can guarantee the specific determination of UA at a very low concentration level regardless of the used fermentation matrix (*e.g.,* yeast or *E.coli* supernatant). In case of absence of UA in fermentation samples no current changes in the basic line of Cu-NPs/UOx/Naf modified electrode can be recorded. In contrast, the pronounced current decrease below the basic line of Cu-NPs/UOx/Naf modified electrode highlights the presence of UA in supernatants and oxidation according to a biochemical route. This current dependency was linear for UA concentrations till 20 μM (negative calibration).

The quantification results of UA in fermentation samples using negative calibration are summarized in Table 3. This table also includes quantification data obtained from the same electrode after heating at 70 °C for 20 min, thus resulting in switching from enzymatic to non-enzymatic read-out. After thermal deactivation of UOx, conventional calibration in UA solutions at low concentrations was achieved (**ESI, Fig. S7B**).

Unexpectedly, the electrode with the electrodeposited Cu-NP/UOx/Naf film after heating showed very similar UA quantification results in fermentation samples to those detected with a fluorescence bioassay (**Table S1**). Moreover, the stability of the intact signal of the electrode modified by Cu-NPs/UOx/Naf was improved after heating from 7-10 days to 4 months. This effect of thermally de-activated UOx in the sensing layer design will be studied in our laboratory in the future. Furthermore, studies should also be extended to testing of alternative non-noble peroxide insensitive electrocatalysts, which could be used in the design of electrodeposited sensing layers for rapid amperometric UA detection.

4. Conclusions

This work introduced a novel conceptual approach to amperometric enzymatic detection of UA at concentrations below 50 μM. Specifically, electrocatalysts frequently used in biosensors design were shown to respond to UA in the absence of specific enzyme at relatively low applied potential (*e.g.,* 0.2 – 0.4 V). Because several concurrent routes are present on the surfaces of noble metal based electrocatalysts, the electrooxidation of UA appears to be superior to biochemical enzymatic reaction. As a solution, a novel strategy for amperometric enzymatic hydrogen peroxide independent UA sensing was proposed.

Table 3
Quantification results for UA in selected supernatants recorded from the tested electrodes by negative and conventional calibration.

Sensing layer	Calibration formula, R^2	UA amount in yeast supernatant (OD = 4.9), μM	UA amount in *E.coli* supernatant (OD = 3.1), μM
Cu-NPs/UOx/Naf (negative calibration)	y = -0.039x + 0.4772, R^2 = 0.971	5.46 ± 0.06	8.36 ± 0.07
Cu-NPs/UOx/Naf after heating (conventional calibration)	y = 0.0046x + 0.0094, R^2 = 0.997	4.39 ± 0.01	9.82 ± 0.01

First, we showed that an ideal UA-sensitive electrocatalysts should exclude the reaction with H_2O_2 as a product of biochemical reaction (*i*). Second, a strategy enabling the electrochemical route to be distinguished from the biochemical reaction recorded from SPE modified by electrodeposited hybrid film was optimized (*ii*). As a case study, the design of an electrode with electrodeposited Cu-NPs/UOx/Naf sensing film was developed (*iii*). Selectivity test with potentially interfering purines, adenine, xanthine and other electroactive substances present in fermentation samples, *e.g.,* ethanol, glycerol or urea, did not reveal any effects on the detection of UA. Finally, an enzymatic quantification strategy for UA based on the negative calibration caused by formation of non-electroactive products of enzymatic reaction was described (*iv*). Quantification test results of UA concentrations in supernatants of yeast and bacterial (*E. coli*) cells were in line with those from Amplex™ Red Uric Acid/Uricase assays.

In summary, this research not only advances the design of UA-sensitive amperometric biosensors as an alternative to peroxide dependent biosensors but also offers new analytical guidelines for studying and validating the activity of electrodeposited enzymes (oxidase). We believe that application of the simple electrodeposited approach used herein for instrumentally controlled synthesis of functional sensing layers based on non-noble metal electrocatalysts and bioorganic compounds will be able to address reproducibility issues in electroanalytical data from electrochemical assays in the future.

CRediT authorship contribution statement

M. Koch: Validation, Methodology, Investigation, Formal analysis. **Y.E. Silina:** Writing – original draft, Validation, Resources, Project administration, Methodology, Funding acquisition, Data curation, Conceptualization.

Declaration of competing interest

The authors declare that they have no known competing financial interests or personal relationships that could have appeared to influence the work reported in this paper.

Acknowledgements

This study was a part of the research program of Y.E.S. funded by the Deutsche Forschungsgemeinschaft (DFG, German Research Foundation, project 427949628).

The authors thank Prof. Dr. E.V. Zolotukhina for advising the range of currents applied for electrodeposition of Cu-NPs and Ni-NPs.

Appendix A. Supplementary data

Supplementary data to this article can be found online at https://doi.

org/10.1016/j.microc.2024.112091.

Data availability

Data will be made available on request.

References

[1] R.M. Hafez, T.M. Abdel-Rahman, R.M. Naguib, Uric acid in plants and microorganisms: Biological applications and genetics - A review, J. Adv. Res. 8 (2017) 475–486, https://doi.org/10.1016/j.jare.2017.05.003.

[2] N. Cooper, R. Khosravan, C. Erdmann, J. Fiene, J.W. Lee, Quantification of uric acid, xanthine and hypoxanthine in human serum by HPLC for pharmacodynamic studies, J. Chromatogr. B Anal. Technol. Biomed. Life Sci. 837 (2006) 1–10, https://doi.org/10.1016/j.jchromb.2006.02.060.

[3] T.M. Blicharz, D.M. Rissin, M. Bowden, R.B. Hayman, C. DiCesare, J.S. Bhatia, N. Grand-Pierre, W.L. Siqueira, E.J. Helmerhorst, J. Loscalzo, F.G. Oppenheim, D. R. Walt, Use of colorimetric test strips for monitoring the effect of hemodialysis on salivary nitrite and uric acid in patients with end-stage renal disease: a proof of principle, Clin. Chem. 54 (2008) 1473–1480, https://doi.org/10.1373/clinchem.2008.105320.

[4] L. Zhang, W. Guo, C. Lv, X. Liu, M. Yang, M. Guo, Q. Fu, Electrochemical biosensors represent promising detection tools in medical field, Adv. Sensor Energy Mater. (2023), https://doi.org/10.1016/j.asems.2023.100081.

[5] S. Masrat, V. Nagal, M. Khan, I. Moid, S. Alam, K.S. Bhat, A. Khosla, R. Ahmad, Electrochemical Ultrasensitive Sensing of Uric Acid on Non-Enzymatic Porous Cobalt Oxide Nanosheets-Based Sensor, Biosensors 12 (2022), https://doi.org/10.3390/bios12121140.

[6] S. Çete, A. Yaşar, F. Arslan, An amperometric biosensor for uric acid determination prepared from uricase immobilized in polypyrrole film, Artificial Cells, Blood Substitutes, and Biotechnology. 34 (2006) 367–380, https://doi.org/10.1080/10731190600684116.

[7] S. Tvorynska, J. Barek, B. Josypčuk, Flow amperometric uric acid biosensors based on different enzymatic mini-reactors: A comparative study of uricase immobilization, Sens. Actuators B 344 (2021), https://doi.org/10.1016/j.snb.2021.130252.

[8] R. Rawal, S. Chawla, N. Chauhan, T. Dahiya, C.S. Pundir, Construction of amperometric uric acid biosensor based on uricase immobilized on PBNPs/cMWCNT/PANI/Au composite, Int. J. Biol. Macromol. 50 (2012) 112–118, https://doi.org/10.1016/j.ijbiomac.2011.10.002.

[9] B. Thakur, S.N. Sawant, Polyaniline/prussian-blue-based amperometric biosensor for detection of uric acid, ChemPlusChem 78 (2013) 166–174, https://doi.org/10.1002/cplu.201200222.

[10] B. Öndeş, S. Evli, Y. Şahin, M. Uygun, D.A. Uygun, Uricase based amperometric biosensor improved by AuNPs-TiS2 nanocomposites for uric acid determination, Microchem. J. 181 (2022), https://doi.org/10.1016/j.microc.2022.107725.

[11] P.E. Erden, E. Kiliç, A review of enzymatic uric acid biosensors based on amperometric detection, Talanta 107 (2013) 312–323, https://doi.org/10.1016/j.talanta.2013.01.043.

[12] J. Luo, J. Cui, Y. Wang, D. Yu, Y. Qin, H. Zheng, X. Shu, H.H. Tan, Y. Zhang, Y. Wu, Metal-organic framework-derived porous Cu2O/Cu@C core-shell nanowires and their application in uric acid biosensor, Appl. Surf. Sci. 506 (2020) 144662, https://doi.org/10.1016/j.apsusc.2019.144662.

[13] S. Verma, J. Choudhary, K.P. Singh, P. Chandra, S.P. Singh, Uricase grafted nanoconducting matrix based electrochemical biosensor for ultrafast uric acid detection in human serum samples, Int. J. Biol. Macromol. 130 (2019) 333–341, https://doi.org/10.1016/j.ijbiomac.2019.02.121.

[14] B. Öndeş, S. Evli, Y. Şahin, M. Uygun, D.A. Uygun, Uricase based amperometric biosensor improved by AuNPs-TiS2 nanocomposites for uric acid determination, Microchem. J. 181 (2022) 107725, https://doi.org/10.1016/j.microc.2022.107725.

[15] R. Jirakunakorn, S. Khumngern, J. Choosang, P. Thavarungkul, P. Kanatharana, A. Numnuam, Uric acid enzyme biosensor based on a screen-printed electrode coated with Prussian blue and modified with chitosan-graphene composite cryogel, Microchem. J. 154 (2020) 104624, https://doi.org/10.1016/j.microc.2020.104624.

[16] W. Liu, Y. Nie, M. Zhang, K. Yan, M. Wang, Y. Guo, Q. Ma, A novel nanosponge–hydrogel system-based electrochemiluminescence biosensor for uric acid detection, Luminescence 37 (2022) 1524–1531, https://doi.org/10.1002/bio.4326.

[17] N.S.K. Gowthaman, M. Amalraj, S. Kesavan, K. Rajalakshmi, S. Shankar, B. Sinduja, P. Arul, R. Karthikeyan, C. Loganathan, V. Mangala Gowri, J. Kappen, A. Ajith, W. Sea Chang, Zero-, one- and two-dimensional carbon nanomaterials as low-cost catalysts in optical and electrochemical sensing of biomolecules and environmental pollutants, Microchemical Journal. 194 (2023) 109291. 10.1016/j.microc.2023.109291.

[18] N.S.K. Gowthaman, B. Sinduja, R. Karthikeyan, K. Rubini, S. Abraham John, Fabrication of nitrogen-doped carbon dots for screening the purine metabolic disorder in human fluids, Biosensors and Bioelectronics. 94 (2017) 30–38. 10.1016/j.bios.2017.02.034.

[19] S. Masrat, V. Nagal, M. Khan, A. Ahmad, M.B. Alshammari, S. Alam, U.T. Nakate, B. Lee, P. Mishra, K.S. Bhat, R. Ahmad, Electrochemical Sensing of Uric Acid with Zinc Oxide Nanorods Decorated with Copper Oxide Nanoseeds, ACS Appl. Nano Mater. 6 (2023) 16615–16624, https://doi.org/10.1021/acsanm.3c02794.

[20] V. Nagal, S. Masrat, M. Khan, S. Alam, A. Ahmad, M.B. Alshammari, K.S. Bhat, S. M. Novikov, P. Mishra, A. Khosla, R. Ahmad, Highly Sensitive Electrochemical Non-Enzymatic Uric Acid Sensor Based on Cobalt Oxide Puffy Balls-like Nanostructure, Biosensors 13 (2023), https://doi.org/10.3390/bios13030375.

[21] V. Nagal, T. Tuba, V. Kumar, S. Alam, A. Ahmad, M.B. Alshammari, A.K. Hafiz, R. Ahmad, A non-enzymatic electrochemical sensor composed of nano-berry shaped cobalt oxide nanostructures on a glassy carbon electrode for uric acid detection, New J. Chem. 46 (2022) 12333–12341, https://doi.org/10.1039/D2NJ01961B.

[22] V. Nagal, V. Kumar, M. Khan, S.Y. AlOmar, N. Tripathy, K. Singh, A. Khosla, N. Ahmad, A.K. Hafiz, R. Ahmad, A highly sensitive uric acid biosensor based on vertically arranged ZnO nanorods on a ZnO nanoparticle-seeded electrode, New J. Chem. 45 (2021) 18863–18870, https://doi.org/10.1039/D1NJ03744G.

[23] V. Nagal, M. Khan, S. Masrat, S. Alam, A. Ahmad, M.B. Alshammari, K.S. Bhat, R. Ahmad, Hexagonal cobalt oxide nanosheet-based enzymeless electrochemical uric acid sensor with improved sensitivity, New J. Chem. 47 (2023) 4206–4212, https://doi.org/10.1039/D2NJ06331J.

[24] S. Knežević, M. Ognjanović, V. Stanković, M. Zlatanova, A. Nešić, M. Gavrović-Jankulović, D. Stanković, La(OH)(3) Multi-Walled Carbon Nanotube/Carbon Paste-Based Sensing Approach for the Detection of Uric Acid-A Product of Environmentally Stressed Cells., Biosensors. 12 (2022). 10.3390/bios12090705.

[25] M. Sun, C. Cui, H. Chen, D. Wang, W. Zhang, W. Guo, Enzymatic and Non-Enzymatic Uric Acid Electrochemical Biosensors: A Review, ChemPlusChem 88 (2023) e202300262.

[26] A. Ajith, N.S.K. Gowthaman, D. Pandiarajan, C. Sugumar, S.A. John, 2-D graphitic carbon nitride fabricated electrode as a robust inexpensive electrochemical scaffold for the real-time detection of serum uric acid in gout patients, Microchem. J. 199 (2024) 110020, https://doi.org/10.1016/j.microc.2024.110020.

[27] E. Katz, V. Privman, J. Wang, Towards biosensing strategies based on biochemical logic systems, 4th International Conference on Quantum, Nano and Micro Technologies, ICQNM 2010. (2010) 1–9. 10.1109/ICQNM.2010.8.

[28] D. Semenova, K.V. Gernaey, B. Morgan, Y.E. Silina, Towards one-step design of tailored enzymatic nanobiosensors, Analyst (2020), https://doi.org/10.1039/c9an01745c.

[29] Y.E. Silina, E.V. Zolotukhina, M. Koch, C. Fink-Straube, A tandem of GC-MS and electroanalysis for a rapid chemical profiling of bacterial extracellular matrix, Electroanalysis (2023) 1–16, https://doi.org/10.1002/elan.202300178.

[30] Y.E. Silina, E.V. Butyrskaya, M. Koch, C. Fink-Straube, N. Korkmaz, M. G. Levchenko, E.V. Zolotukhina, Mechanistic aspects of glycerol oxidation on palladium electrocatalysts in model aqueous and fermentation media solutions, Electrochim. Acta (2024) 144479, https://doi.org/10.1016/j.electacta.2024.144479.

[31] D. Semenova, Y.E. Silina, The Role of Nanoanalytics in the Development of Organic-Inorganic Nanohybrids—Seeing Nanomaterials as They Are, Nanomaterials 9 (2019), https://doi.org/10.3390/nano9121673.

[32] Y.E. Silina, One-step electrodeposited hybrid nanofilms in amperometric biosensor development, Anal. Methods 16 (2024) 2424–2443, https://doi.org/10.1039/D4AY00290C.

[33] K. Pontius, D. Semenova, Y.E. Silina, K.V. Gernaey, H. Junicke, Automated Electrochemical Glucose Biosensor Platform as an Efficient Tool Toward On-Line Fermentation Monitoring: Novel Application Approaches and Insights, Front. Bioeng. Biotechnol. 8 (2020) 1–15, https://doi.org/10.3389/fbioe.2020.00436.

[34] D. Semenova, Y.E. Silina, M. Koch, L. Micheli, A. Zubov, K.V. Gernaey, Sensors for biosensors: A novel tandem monitoring in a droplet towards efficient screening of robust design and optimal operating conditions, Analyst (2019), https://doi.org/10.1039/c8an02261e.

[35] C.L. Benn, P. Dua, R. Gurrell, P. Loudon, A. Pike, R. Ian Storer, C. Vangjeli, Physiology of hyperuricemia and urate-lowering treatments, Front. Med. 5 (2018) 1–28, https://doi.org/10.3389/fmed.2018.00160.

[36] D.P. Chong, Theoretical Study of Uric Acid and its Ions in Aqueous Solution, Journal of Theoretical and Computational, Science 1 (2013) 1–7, https://doi.org/10.4172/jtco.1000104.

[37] M. Koch, N. Apushkinskaya, E.V. Zolotukhina, Y.E. Silina, Towards hybrid one-pot/one-electrode Pd-NPs-based nanoreactors for modular biocatalysis, Biochem. Eng. J. 175 (2021) 108132, https://doi.org/10.1016/j.bej.2021.108132.

[38] P. Pfrimer, L.M.P. de Moraes, A.S. Galdino, L.P. Salles, V.C.B. Reis, J.L. De Marco, M.V. Prates, C. Bloch Jr., F.A.G. Torres, Cloning, Purification, and Partial Characterization of Bacillus subtilis Urate Oxidase Expressed in Escherichia coli, Biomed Res. Int. 2010 (2010) 674908, https://doi.org/10.1155/2010/674908.

[39] H. Tian, Y. Guo, X. Gao, W. Yao, PEGylation enhancement of pH stability of uricase via inhibitive tetramer dissociation, J. Pharm. Pharmacol. 65 (2013) 53–63, https://doi.org/10.1111/j.2042-7158.2012.01575.x.

[40] Y.E. Silina, N. Apushkinskaya, N.V. Talagaeva, M.G. Levchenko, E.V. Zolotukhina, Electrochemical operational principles and analytical performance of Pd-based amperometric nanobiosensors, Analyst 146 (2021) 4873–4882, https://doi.org/10.1039/D1AN00882J.

[41] E.V. Zolotukhina, E.V. Butyrskaya, C. Fink-Straube, M. Koch, Y.E. Silina, Towards controlled and simple design of non-enzymatic amperometric sensor for glycerol determination in yeast fermentation medium, Anal. Bioanal. Chem. 416 (2024) 3619–3630, https://doi.org/10.1007/s00216-024-05316-7.

[42] Y.E. Silina, E.V. Zolotukhina, M. Koch, C. Fink-Straube, A tandem of GC-MS and electroanalysis for a rapid chemical profiling of bacterial extracellular matrix, Electroanalysis 35 (2023) e202300178.

[43] T.-H. Yin, B.-J. Liu, Y.-W. Lin, Y.-S. Li, C.-W. Lai, Y.-P. Lan, C. Choi, H.-C. Chang, Y. Choi, Electrodeposition of Copper Oxides as Cost-Effective Heterojunction

Photoelectrode Materials for Solar Water Splitting, Coatings 12 (2022), https://doi.org/10.3390/coatings12121839.
[44] N. Zurita, S.G. García, Comparative study of electrodeposited copper nanoparticles on different substrates for their use in the reduction of nitrate ions, Results Eng. 17 (2023) 100800, https://doi.org/10.1016/j.rineng.2022.100800.
[45] Q. Liu, M.M. Maroto-Valer, Studies of pH buffer systems to promote carbonate formation for CO2 sequestration in brines, Fuel Process. Technol. 98 (2012) 6–13, https://doi.org/10.1016/j.fuproc.2012.01.023.